Supporting Material for: Giant mechanocaloric effects in fluorite-structured superionic materials

Claudio Cazorla*

School of Materials Science and Engineering,

UNSW Australia, Sydney NSW 2052, Australia

Integrated Materials Design Centre,

UNSW Australia, Sydney NSW 2052, Australia

Daniel Errandonea

Departamento de Física Aplicada (ICMUV), Malta Consolider Team,

Universitat de Valencia, 46100 Burjassot, Spain

Abstract

In this supplemental document we explain the details of our classical molecular dynamics and density functional theory calculations performed in CaF_2 and PbF_2 under hydrostatic, biaxial, and uniaxial stress conditions. Special emphasis is put on the computation of the isothermal entropy, ΔS, and adiabatic temperature, ΔT, changes induced by varying stresses. Also, we report the structural and energy results calculated with first-principles methods in both fluorite-structured superionic materials, and the heat capacity and strain curves obtained with classical molecular dynamics.

I. CLASSICAL MOLECULAR DYNAMICS SIMULATIONS

The interatomic potential adopted in this study is $U(r) = V_{\mathrm{A-F}}(r) + V_{\mathrm{F-F}}(r) + V_{\mathrm{A-A}}(r)$, where $\mathrm{A} = \mathrm{Ca}, \mathrm{Pb}$ and terms V_{ij} are of the Born-Mayer-Huggins (BMH) form (see Eq. 1). Each pairwise term is composed of three different contributions; the first is of exponential type and accounts for the short-ranged atomic repulsion deriving from the overlapping between different electron clouds; the second term is proportional to r^{-6}, with r being the radial distance between a pair of ions, and represents the long-ranged atomic attraction due to dispersive van der Waals forces; the third term is the usual Coulomb interaction between puntual atomic charges, which in our case are taken to be $Z_{\mathrm{A}} = +2e$ and $Z_{\mathrm{F}} = -1e$. In Table I, we enclose the value of the BMH parameters that have been used throughout this work to simulate CaF_2 [1] and PbF_2 [2].

$$V_{ij}(r) = A_{ij} e^{-\frac{r}{\rho_{ij}}} - \frac{C_{ij}}{r^6} + \frac{Z_i Z_j}{r} \tag{1}$$

Comprehensive one-phase (N, P, T) molecular dynamics simulations were carried out in order to compute the superionic transition temperature in cubic CaF_2 and PbF_2 as a function of stress. Calculations comprised large simulation boxes of $6,144$ atoms and long simulation times of ~ 100 ps, thus ensuring that the results were free of size-effect bias and guaranteeing thermodynamic consistency (e.g. well-defined energies, equality of the three diagonal components and nullity of all off-diagonal components of the stress tensor). We systematically carried out simulations at temperature intervals of 100 K up to $T_s + 300$ K at each σ point considered.

Following previous works [3–6], we identified superionicity through inspection of the time-dependent mean squared displacement function (MSD) obtained in one-phase MD simulations. The MSD function is defined as

$$\langle \Delta R_i^2(t) \rangle = \langle |R_i(t + t_0) - R_i(t_0)|^2 \rangle \ , \tag{2}$$

where $R_i(t)$ is the position of ion i at time t, t_0 is an arbitrary time origin, and $\langle \cdots \rangle$ denotes time average. $\langle \Delta R_i^2(t) \rangle$ was computed separately for each type of ions and time averages were performed over t_0, that is, every sample point in the simulation was used as a new time origin. F^- diffusion is signaled in practice by the appearance of a non-zero MSD slope, as it is shown in Fig. 1.

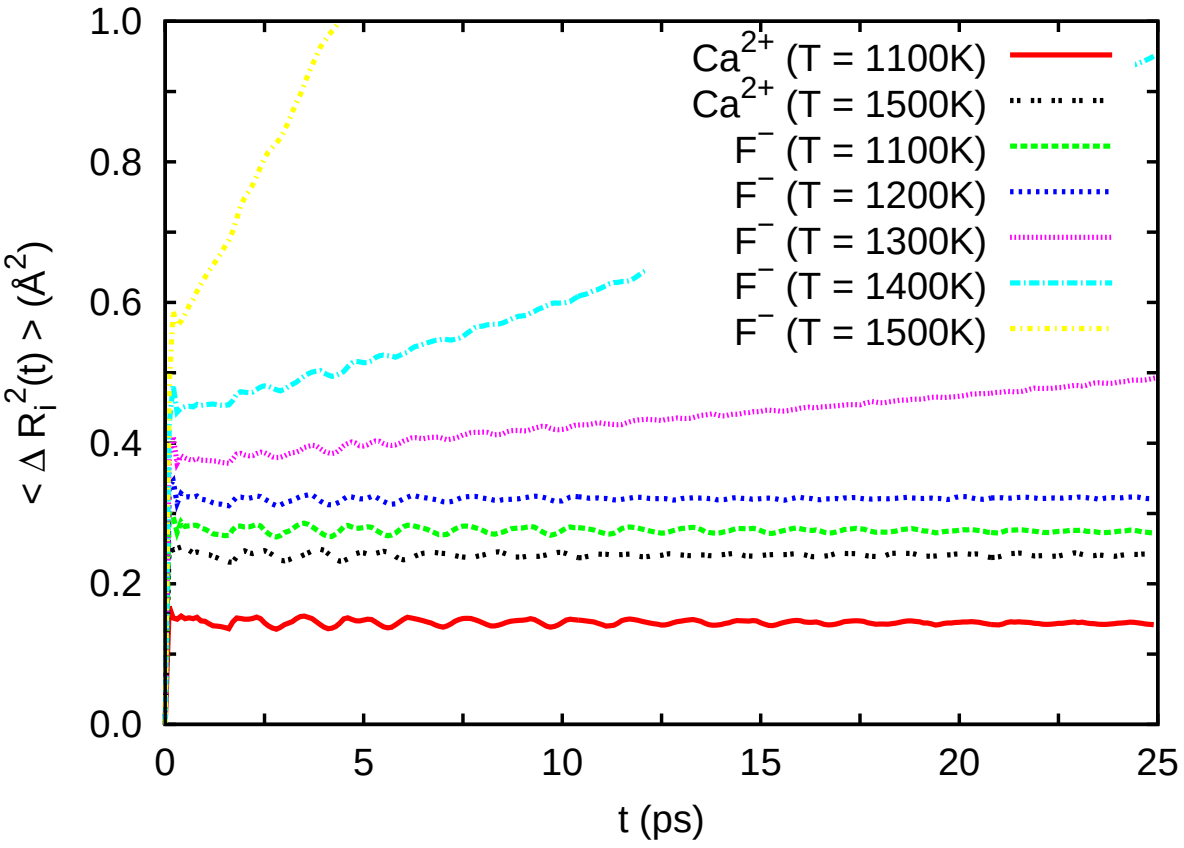

FIG. 1: [Supplemental] Mean squared displacement of fluorine and calcium ions in CaF_2 represented as a function of time at temperatures above and below the corresponding transition point T_s = 1350(50) K at $\sigma = 0$ conditions.

II. *AB INITIO* MOLECULAR DYNAMICS SIMULATIONS

Ab initio molecular dynamics (AIMD) simulations based on density functional theory were performed in the canonical (N, V, T) ensemble for CaF_2 and PbF_2. The temperature in the simulations was kept fluctuating around a set-point value by using Nose-Hoover thermostats. Large simulation boxes containing 192 atoms were used in all the cases, and periodic boundary conditions were applied along the three corresponding Cartesian directions. Newton's equations of motion were integrated using the customary Verlet's algorithm and a time-step length of 10^{-3} ps. Γ-point sampling for integration within the first Brillouin zone was employed in all the AIMD simulations. Calculations comprised long simulation times of up to $\sim$ 30 ps. Our AIMD simulations were carried out systematically at temperature intervals of 250 K up to $T_s + 500$ K at each considered volume.

	A (eV)	ρ (Å)	C (eV Å^6)
		CaF_2	
$Ca-F$	1717.441	0.287	0.102
$F-F$	2058.994	0.252	16.703
$Ca-Ca$	0.0	0.0	0.0
		PbF_2	
$Pb-F$	122.700	0.516	0.000
$F-F$	10225.0	0.225	107.3
$Pb-Pb$	0.0	0.0	0.0

TABLE I: Interatomic pair potential parameters used to describe CaF_2 [1] and PbF_2 [2] in the classical molecular dynamics simulations.

Consistently, superionicity was identified through inspection of the time-dependent mean squared displacement function obtained in the AIMD runs (see Sec. I and Fig. 2). To ascertain that the crystal remained vibrationally stable (i.e., the thermal average position of each ion remains centered on its perfect-lattice site), we computed also the position correlation function defined as:

$$p(t) \equiv \langle [R_i(t+t_0) - R_i^0] \cdot [R_i(t_0) - R_i^0] \rangle \ , \tag{3}$$

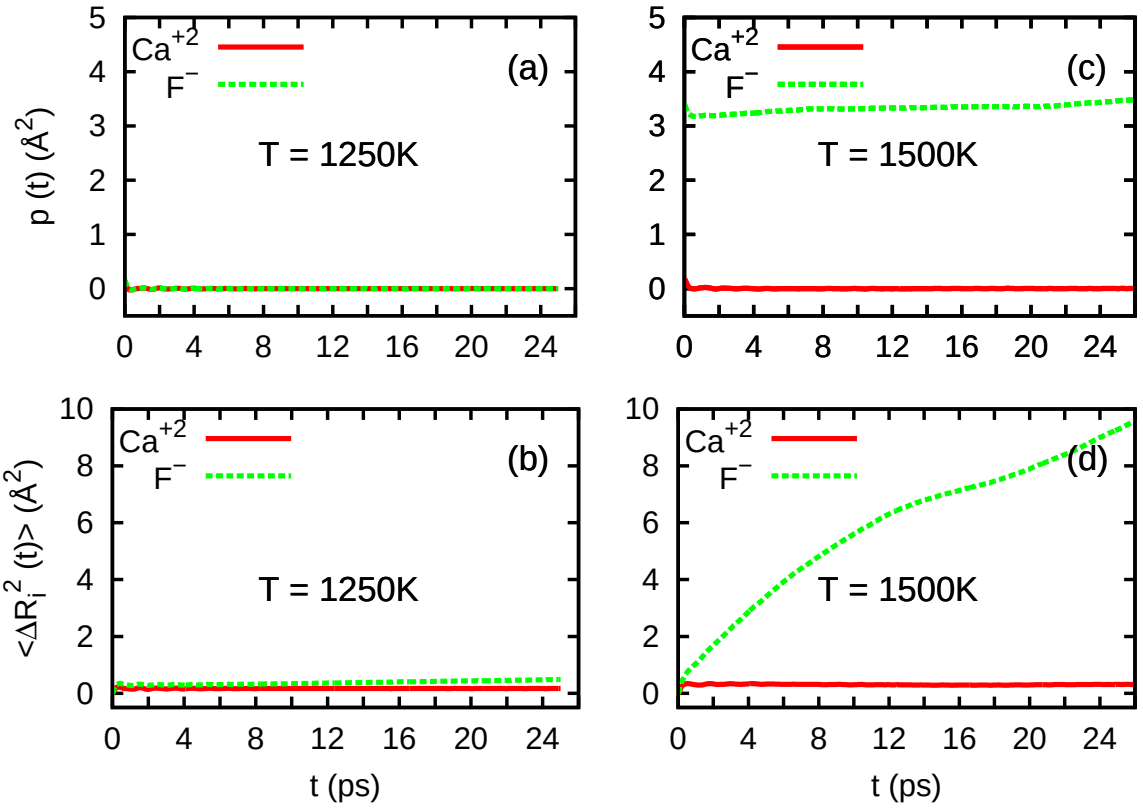

FIG. 2: [Supplemental] Calculated position correlation function and mean squared displacement in CaF_2 at $T = 1250$ K (a)-(b) and 1500 K (c)-(d) [$\sigma \sim 0$ GPa] using *ab initio* molecular dynamics simulations based on density functional theory.

where $R_i(t)$ is the position of ion i at time t, R_i^0 the corresponding perfect-lattice position, t_0 an arbitary time origin, and $\langle\cdot\rangle$ denotes thermal average (see Fig. 2) [7,8]. The crystal is vibrationally stable if $p(t \to \infty) = 0$ because the displacements at widely separated times become uncorrelated. On the contrary, if the atoms acquire a permanent vibrational displacement, $p(t \to \infty)$ becomes non-zero. In the AIMD simulations performed in CaF_2 and PbF_2, we found that the crystals always remained vibrationally stable in the normal (or non-superionic) state, that is, $p(t \to \infty) = 0$, within the considered σ intervals.

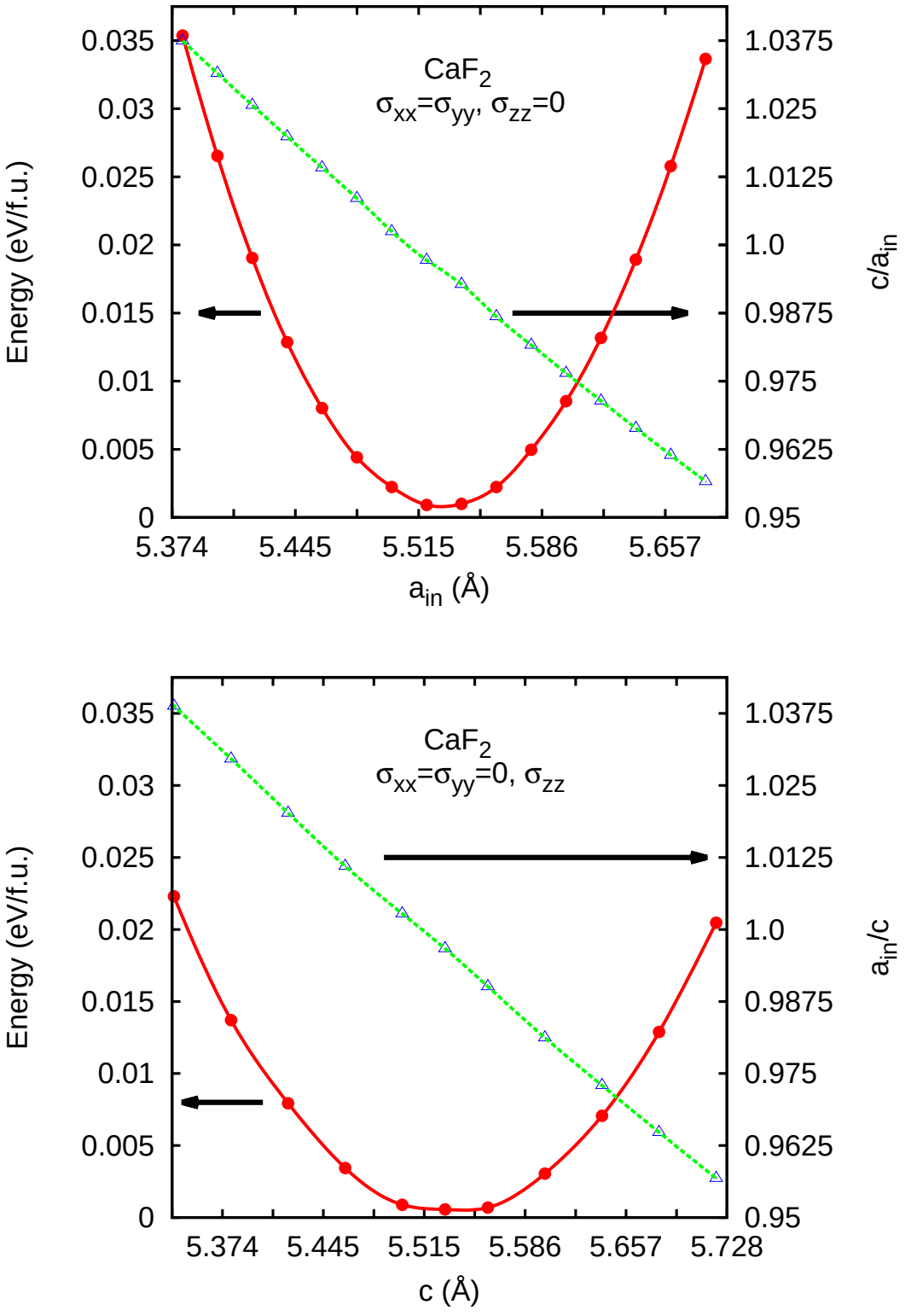

FIG. 3: [Supplemental] (*Top*) Density functional theory results obtained in CaF_2 at $T = 0$ K and considering both compressive and tensile biaxial stresses. (*Bottom*) Idem as above but considering compressive and tensile uniaxial stresses.

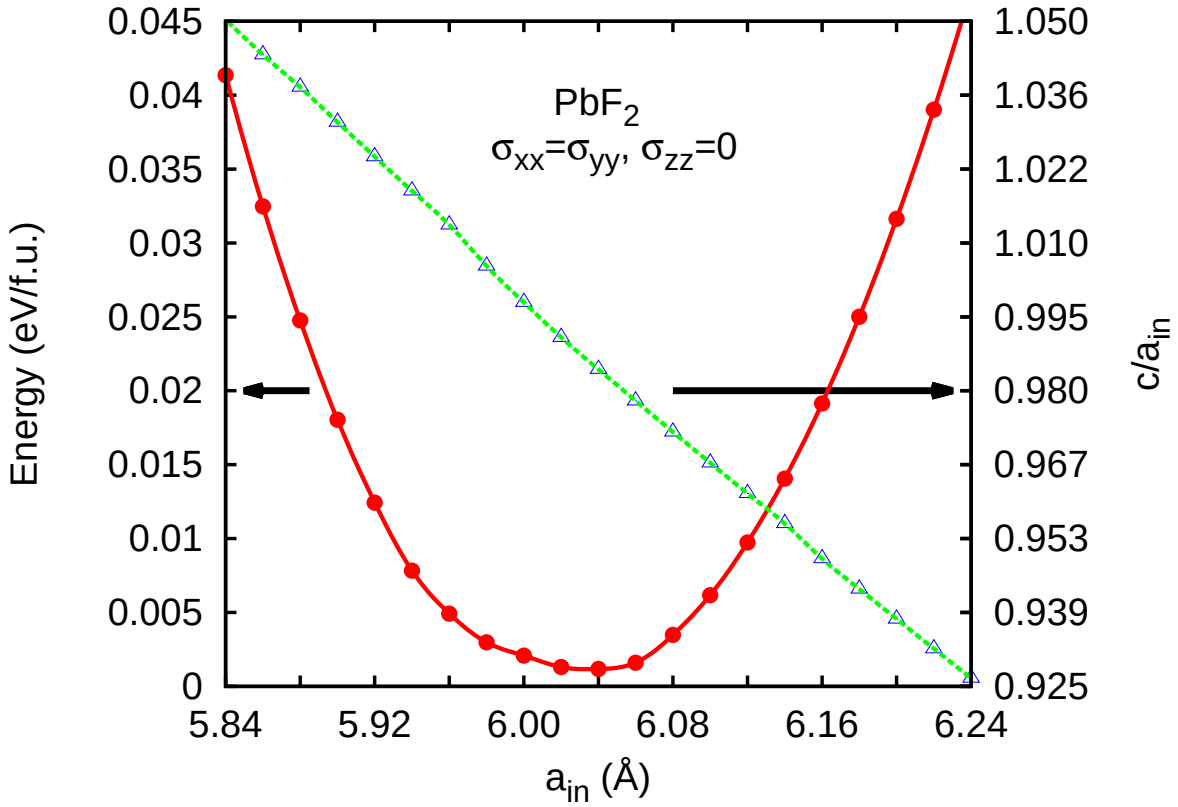

FIG. 4: [Supplemental] Density functional theory results obtained in PbF_2 at $T = 0$ K and considering both compressive and tensile biaxial stresses.

III. ZERO TEMPERATURE RESULTS OBTAINED WITH FIRST-PRINCIPLES METHODS

The ground-state structure of both CaF_2 and PbF_2 is the cubic fluorite phase (i.e., $a = b = c$ and $\alpha = \beta = \gamma = 90°$), which is characterised by the space group $Fm\bar{3}m$ and Wyckoff positions $4a$ (Ca^{2+}) and $8c$ (F^-). According to our DFT calculations, the corresponding equilibrium lattice parameters are $a_0 = 5.52$ and 6.03 Å, respectively (see Figs. 3-4). In Figs. 3 and 4, we show the energy and structural DFT results obtained in CaF_2 and PbF_2 considering biaxial and uniaxial stress conditions. Under hydrostatic stress conditions, the three lattice vectors are elongated or reduced a same amount depending on whether σ is negative or positive, and thus the cubic lattice symmetry is preserved (that is, $a = b = c$ and $\alpha = \beta = \gamma = 90°$). Under biaxial (uniaxial) stress conditions, however, the lattice vectors fulfill the relations $a = b \neq c$ ($a = b \neq c$) and $c > a$ ($c < a$) or $c < a$ ($c > a$) depending on

whether σ is compressive or tensile (see Fig. 3). In these two latter cases, the symmetry of the crystal transforms into tetragonal and the corresponding space group is $I4/mmm$ (with Wyckoff positions $2a$ [Ca^{2+}] and $4d$ [F^-]), as the three lattice vectors remain orthogonal.

IV. COMPUTATION OF ΔS AND ΔT

The isothermal entropy changes, ΔS, calculated in fluorite-structured FIC at $\sigma < 0$ conditions were obtained with the formulas,

$$\begin{aligned}\Delta S(\sigma_f, T) &= V_0 \cdot \int_0^{|\sigma_f|} \left(\frac{\partial \epsilon_{zz}}{\partial T}\right)_\sigma d\sigma_{zz} \text{ [uniaxial]}, \\ &= V_0 \cdot \int_0^{|\sigma_f|} \left(\frac{\partial \epsilon_{xx}}{\partial T}\right)_\sigma d\sigma_{xx} + \left(\frac{\partial \epsilon_{yy}}{\partial T}\right)_\sigma d\sigma_{yy} \text{ [biaxial], and} \\ &= V_0 \cdot \int_0^{|\sigma_f|} \left(\frac{\partial \epsilon_{xx}}{\partial T}\right)_\sigma d\sigma_{xx} + \left(\frac{\partial \epsilon_{yy}}{\partial T}\right)_\sigma d\sigma_{yy} + \left(\frac{\partial \epsilon_{zz}}{\partial T}\right)_\sigma d\sigma_{zz} \text{ [hydrostatic]}. \quad (4)\end{aligned}$$

In the equations above, $V_0(T) \equiv L_{x,0}(T) \cdot L_{y,0}(T) \cdot L_{z,0}(T)$ is the T-dependent volume of the cubic system at equilibrium (i.e., considering $\sigma = 0$ conditions), where $L_{i,0}$ represents the length of the simulation box along the i Cartesian direction, and the mechanical strain components are defined as $\epsilon_{ii}(\sigma, T) \equiv \frac{L_i(\sigma,T) - L_{i,0}(T)}{L_{i,0}(T)}$. Because of the cubic symmetry of the crystals under study, ϵ_{xx} and ϵ_{yy} are identical in the biaxial stress case and $\epsilon_{xx} = \epsilon_{yy} = \epsilon_{zz}$ in the hydrostatic stress case.

We note that the ΔS expression employed here for hydrostatic stress calculations is formally equivalent to

$$\Delta S = \int_0^{|P_f|} \left(\frac{\partial V}{\partial T}\right)_P dP \qquad (P \equiv \frac{\sigma_{xx} + \sigma_{yy} + \sigma_{zz}}{3}), \quad (5)$$

which is valid for any crystal symmetry [9]. This can be seen by considering that relation $\frac{\partial V}{\partial T} = 3V_0 \cdot \frac{\partial \epsilon}{\partial T} + \mathcal{O}(\epsilon^2)$ is fulfilled by cubic systems.

With regard to the calculation of the adiabatic temperature changes, ΔT, these were obtained through the expression

$$\Delta T(\sigma_f, T) = -\int_0^{|\sigma_f|} \frac{T}{C_\sigma(\sigma, T)} \cdot dS \ , \quad (6)$$

where $C_\sigma(\sigma, T)$ is the heat capacity of the crystal at fixed σ and which depends on both thermodynamic quantities σ and T.

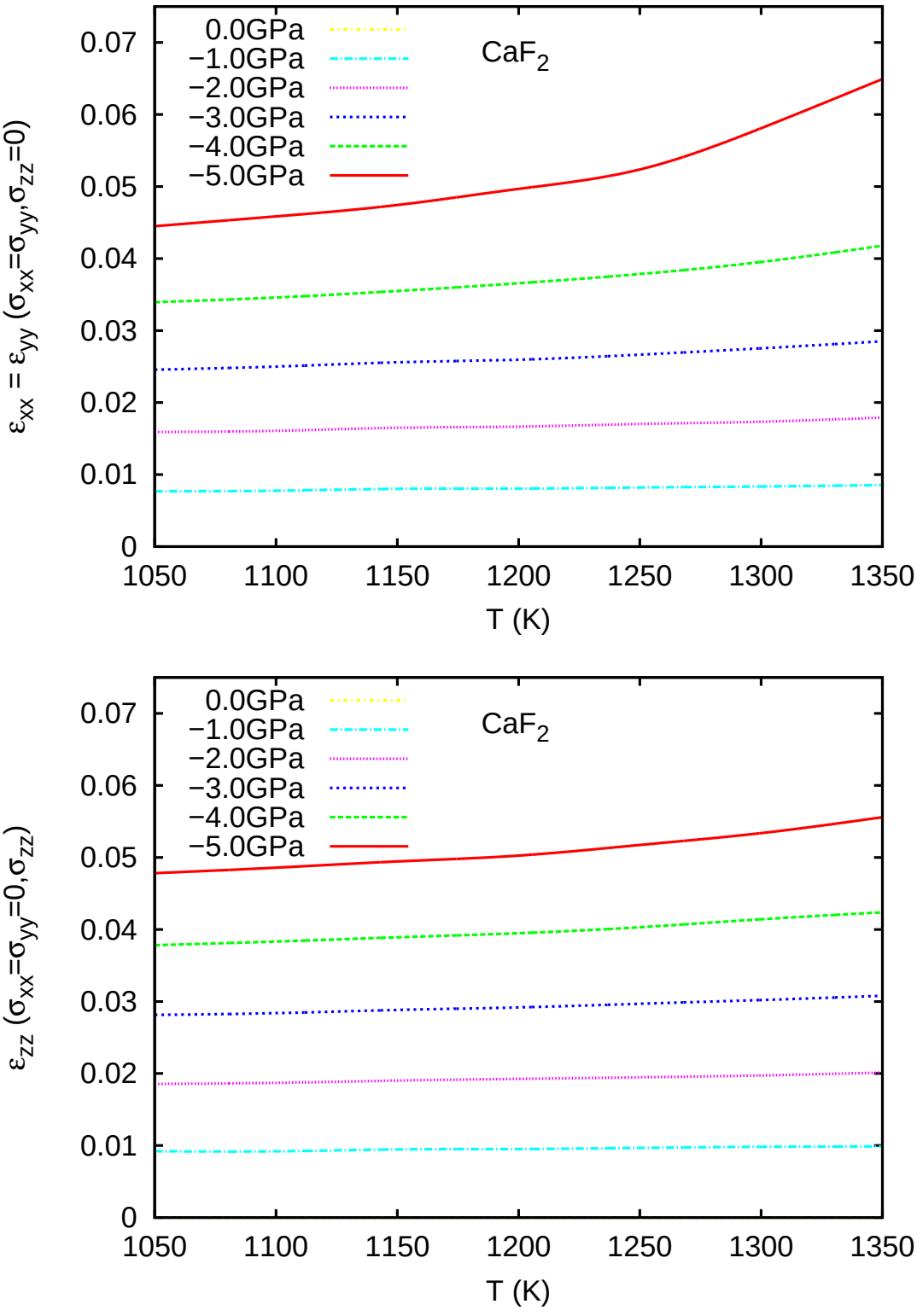

FIG. 5: [Supplemental] (*Top*) Mechanical strains calculated in CaF_2 at different biaxial tensile and temperature conditions, using molecular dynamics simulations. (*Bottom*) Idem as above but considering uniaxial tensile stresses.

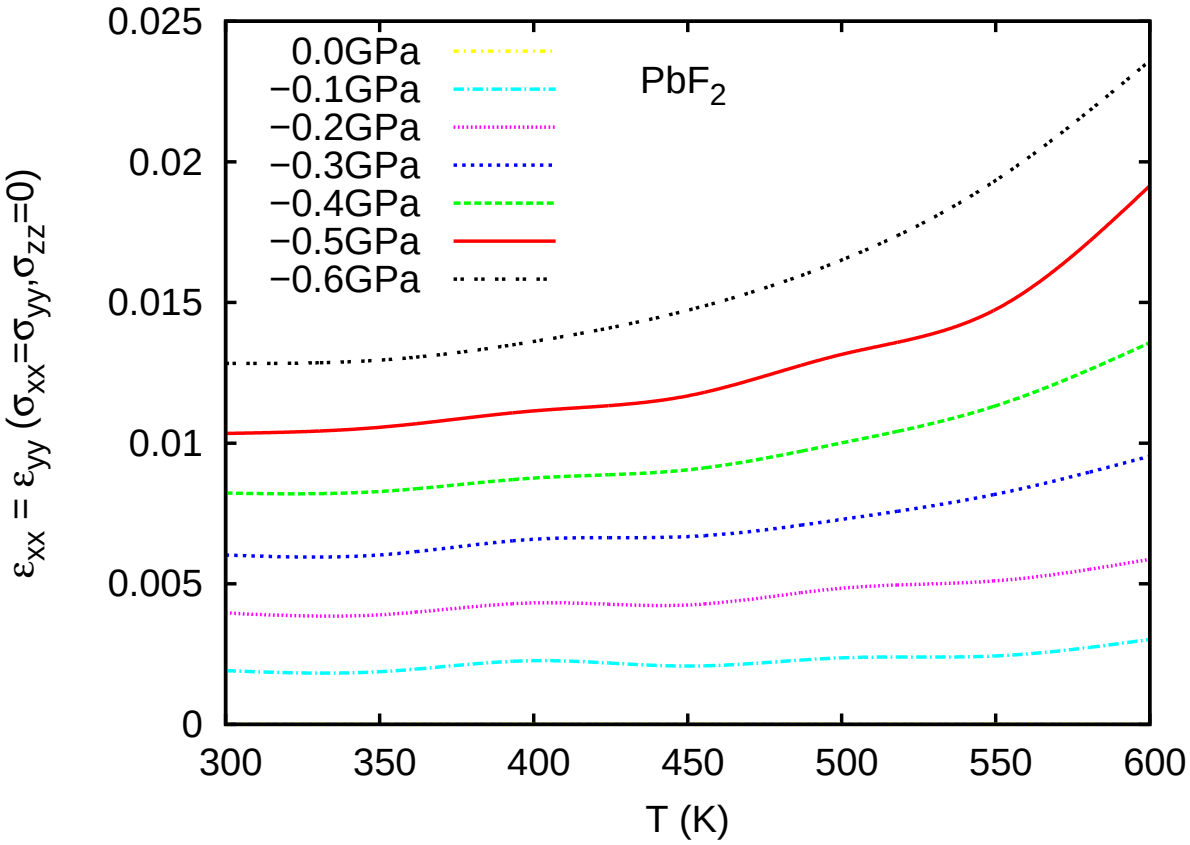

FIG. 6: [Supplemental] Mechanical strains calculated in PbF_2 at different biaxial tensile and temperature conditions, using molecular dynamics simulations.

In order to accurately compute $\Delta S(\sigma, T)$ and $\Delta T(\sigma, T)$ in CaF_2 and PbF_2, we calculated the corresponding mechanical strains and heat capacities in a dense grid of (σ, T) points spaced by $\Delta\sigma = 0.1$ GPa and $\Delta T = 20$ K. Mechanical strains were estimated directly from the MD simulations and the heat capacity from the differences between the internal energies of simulations performed at T and $T \pm 20$ K conditions. Spline interpolations were subsequently applied to the calculated data points in order to obtain continuous and well-behaved $\epsilon(\sigma, T)$ and $C_\sigma(\sigma, T)$ functions (see Figs. 5-7 for some examples). Figure 7 shows some of the calculated $C_\sigma(\sigma, T)$ curves in CaF_2 and PbF_2. At $\sigma = 0$ conditions, the heat capacity starts to increase more noticeably beyond the onset temperature of F^- diffusivity, that is, 1350(50) K in CaF_2 and 650(50) K in PbF_2, which we have identified here as the critical temperature of the normal $\rightarrow$ superionic transition. When tensile stresses are applied, the main peak in the heat capacity is broadened and shifted towards lower temperatures.

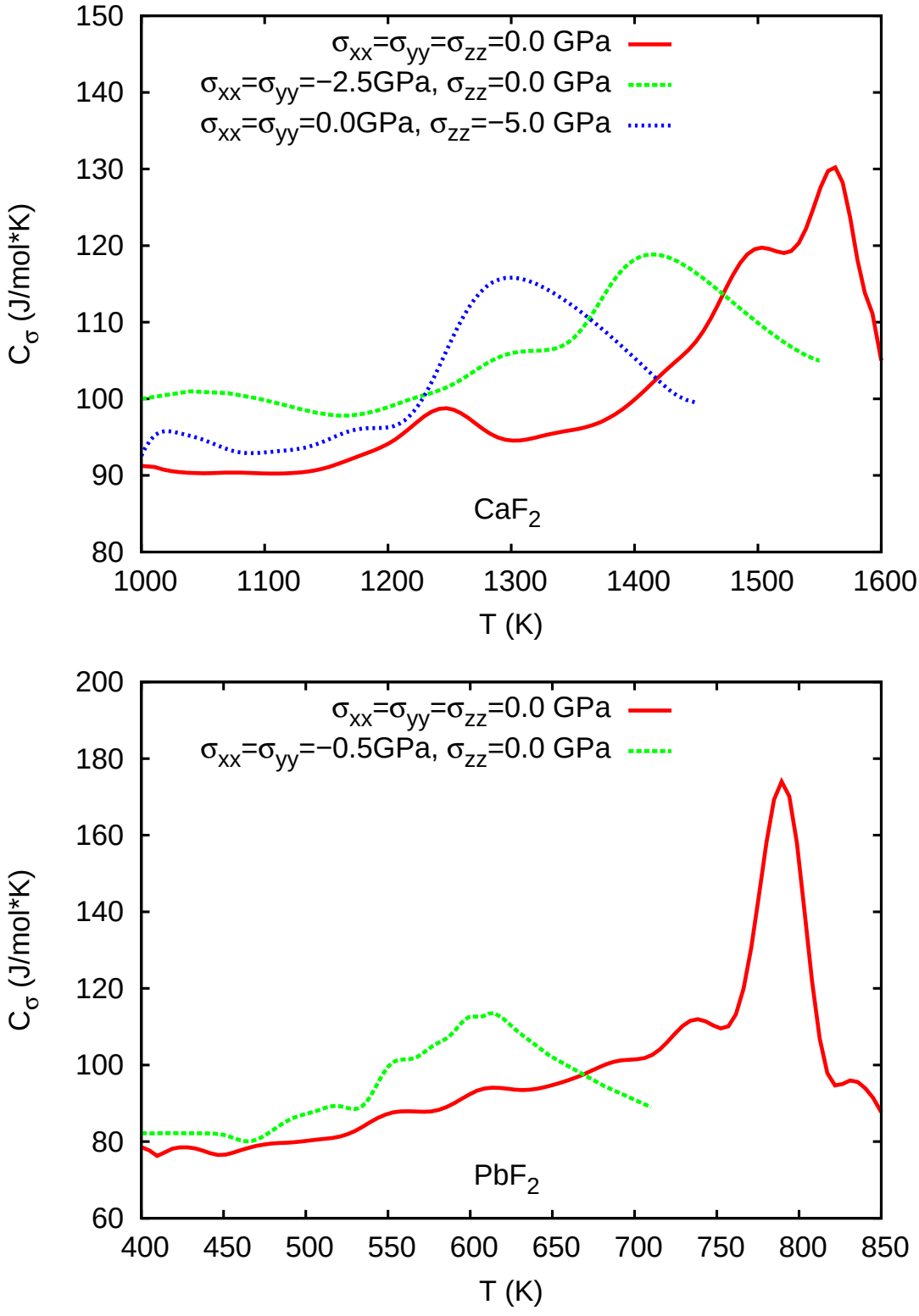

FIG. 7: [Supplemental] (*Top*) Heat capacity calculated in CaF_2 under different stress and temperature conditions, using molecular dynamics simulations. (*Bottom*) Heat capacity calculated in PbF_2 under different stress and temperature conditions, using molecular dynamics simulations.

We note that the differences with respect to the C_σ results obtained at $\sigma = 0$ conditions are quite similar in both the uniaxial and biaxial cases (see top panel in Fig 7). The ΔS and ΔT values shown in Figs. 3 and 4 of the manuscript were obtained by numerically integrating functions $\epsilon(\sigma, T)$ and $C_\sigma(\sigma, T)$ according to Eqs. (4-6), and thus all possible sources of variation were consistently included in our calculations.

---

* Electronic address: c.cazorla@unsw.edu.au; Corresponding Author

[1] C. Cazorla and D. Errandonea, J. Phys. Chem. C **117**, 11292 (2013).

[2] A. B. Walker, M. Dixon, and M. J. Gillan, J. Phys. C: Sol. Stat. Phys. **15**, 4061 (1982).

[3] M. J. Gillan, J. Phys. C: Sol. Stat. Phys. **19**, 3391 (1986); J. Chem. Soc. Faraday Trans. **86**, 1177 (1990).

[4] P. J. D. Lindan and M. J. Gillan, J. Phys.:Condens. Matt. **5**, 1019 (1993).

[5] W.-G. Yin, J. Liu, C.-G. Duan, W. N. Mei, R. W. Smith, and J. R. Hardy, Phys. Rev. B **70**, 064302 (2004).

[6] C. M. Araújo, A. Blomqvist, R. H. Scheicher, P. Chen, and R. Ahuja, Phys. Rev. B **79**, 172101 (2009).

[7] C. Cazorla, D. Alfè, and M. J. Gillan, Phys. Rev. B **85**, 064113 (2012).

[8] L. Vočadlo, D. Alfè, M. J. Gillan, I. G. Wood, J. P. Brodholt, and G. D. Price, Nature (London) **424**, 536 (2003).

[9] X. Moya, S. Kar-Narayan, and N. D. Mathur, Nature Mat. **13**, 439 (2014).